JOURNAL OF AIRCRAFT
Vol. 42, No. 4, July–August 2005

Worst-Case Gust-Response Analysis for Typical Airfoil Section with Control Surface

Atsushi Kanda*
Japan Aerospace Exploration Agency, Tokyo 181-0015, Japan
and
Earl H. Dowell†
Duke University, Durham, North Carolina 27708-0300

This paper determines the worst-case gust response of a typical airfoil section with a control surface. Matched filter theory is employed in order to compute the gust that produces a maximum response. These results are compared with a tuned one-minus-cosine gust, one of the standard representations of discrete gusts. It is found that the responses obtained by the matched filter theory are about twice as large as those obtained using the one-minus-cosine gust. Moreover, it is found that the hinge stiffness of the control surface can affect the plunging motion.

Nomenclature

b	=	length of half-chord
$\boldsymbol{b}$	=	aerodynamic force vector caused by the gust, $(1/\bar{w}_G)\{\bar{L}^G \;\; \bar{M}_\alpha^G \;\; \bar{M}_\beta^G\}^T$
$C(k)$	=	Theodorsen function
$G(s)$, $G(\omega)$	=	gust prefilter
H	=	gust gradient distance
H_h, H_α, H_β	=	transfer functions relating the displacements h, α, β to w_G
$H_y(\omega)$	=	frequency response function of airplane
h	=	plunge displacement, $2bn$
$h_y(t)$	=	unit impulse response
I_α, I_β	=	mass moment of inertia about elastic axis, control surface hinge
$J_0(k)$, $J_1(k)$	=	Bessel function of the first kind
K	=	arbitrary constant
k	=	reduced frequency, $\omega b/U$
L	=	scale of turbulence
L^G	=	lift caused by gust
L^M	=	lift caused by wing motion
L_C^M, L_{NC}^M	=	lift of the circulatory flow, noncirculatory flow
M_α^G, M_β^G	=	moment caused by gust
M_α^M, M_β^M	=	moment caused by wing motion
m	=	airfoil total mass
n	=	gust gradient distance in chords
p, s	=	Laplace variable
R	=	ratio of standard deviations
S_α, S_β	=	static moment
T_i	=	aerodynamic coefficient
t	=	time
t_0, τ_0	=	arbitrary time shift
U	=	airspeed
w_G	=	upwash caused by gust
$w_{0.75c}$	=	downwash at 75% chord
$\hat{w}_{1-\cos}$	=	maximum velocity of discrete gust
x, $X(\omega)$	=	arbitrary input
$\bar{\boldsymbol{x}}$	=	displacement vector, $\{\bar{h} \;\; \bar{\alpha} \;\; \bar{\beta}\}^T$
x^*, ξ^*	=	dimensionless chordwise variable
y, $Y(\omega)$	=	response of linear system
$y_{\max}$	=	maximum response of y
α	=	angle of attack
β	=	deflection angle of control surface at hinge
$\Delta\bar{p}_a$	=	lift distribution caused by gust
$\delta(\tau)$	=	Dirac delta function
ρ	=	air density
σ	=	standard deviation
σ_{h_y}	=	standard deviation of impulse response
σ_x	=	standard deviation of matched excitation waveform
τ	=	nondimensional time, Ut/b
$\Phi(\omega)$	=	von Kármán gust power spectral density
$\phi(\tau)$	=	Wagner function
$\psi(\tau)$	=	Küssner function
ω	=	circular frequency
ω_h, ω_α, ω_β	=	natural circular frequency, given by $\sqrt{(K_h/m)}$, $\sqrt{(K_\alpha/I_\alpha)}$, $\sqrt{(K_\beta/I_\beta)}$

Introduction

TO determine worst-case gust responses is very important for the design and structural safety of aircraft. There are two approaches to compute gust responses. One is a frequency-domain approach, and the power-spectral-density method has been widely used.[1–4] Another approach is a time-domain simulation, which can calculate time-correlated gust responses. This latter approach is, moreover, divided into an optimal search or a deterministic procedure. The statistical-discrete-gust (SDG) method[5,6] belongs to the former procedure and was developed by Jones, whereas the matched filter theory (MFT) is based on the latter procedure. MFT can solve directly for the worst-case gust input without using the calculus of variations and reduces computational costs relative to the SDG method. MFT was applied to an electrical circuit system by Papoulis[7] and implemented to obtain the worst-case gust responses by Zeiler and Pototzky[8] and Pototzky et al.[9]

Most studies of the MFT have been made for gust loads[10–15] except for the study of a plunging motion of a rigid airplane by Lee and Lan.[15] As described in Ref. 9, however, the use of MFT is not limited to gust loads and can be applied for various system outputs. From the viewpoint of passenger comfort, dynamic aircraft motion also becomes important. This paper focuses on gust motion responses instead of gust loads. One purpose of this paper is to apply the MFT to determine the motion of a typical airfoil section with

Received 10 March 2004; revision received 12 July 2004; accepted for publication 15 July 2004.

*Senior Researcher, Institute of Space Technology and Aeronautics. 6-13-1 Osawa, Mitaka. Member AIAA.

†William Holland Hall Professor, Department of Mechanical Engineering and Materials Science. Honorary Fellow AIAA.

a control surface and verify its effectiveness. The MFT results are also compared with responses obtained by the one-minus-cosine discrete gust. The latter is often used to determine discrete dynamic gust loads and is the basis of the SDG method.

Another purpose is to investigate the effects of the hinge stiffness of the control surface on gust responses as an application of the MFT. Control surfaces are often employed for gust load alleviation.[16,17] Similarly, gust motion response can also be controlled by the control surfaces.

Theoretical Development

The basic concept of the MFT is illustrated in Fig. 1. The system dynamics are assumed to be known and are composed of the prefilter and the airplane dynamics. The MFT is a method to obtain the worst-case gust response given these dynamics. The matched excitation waveform, which produces a maximum response, is directly given by a shift and reversal in time from the impulse response of the known system dynamics. The gust input for the airplane is represented by the critical gust profile, which is the response of the prefilter to the matched excitation waveform. Then, the gust response to the matched excitation waveform can be obtained as the worst-case gust response. In the MFT method, searching procedures and the calculus of variations are not needed, unlike the SDG method.

The following mathematical formulation to obtain the maximum gust response by the MFT is summarized from Ref. 9. The response of a linear system $Y(\omega)$ to an arbitrary input $X(\omega)$ in the frequency domain is given by

$$Y(\omega) = H_y(\omega)X(\omega) \tag{1}$$

where $H_y(\omega)$ can be written as

$$H_y(\omega) = G(\omega)H(\omega) \tag{2}$$

The prefilter depends on the problem and should be appropriately selected. For gust-response problems, the von Kármán gust prefilter is generally used. This prefilter is related to the von Kármán gust power spectral density.

The unit impulse response of the system dynamics is, by the inverse Fourier transform,

$$h_y(t) = \frac{1}{2\pi}\int_{-\infty}^{\infty} H_y(\omega)e^{i\omega t}\,\mathrm{d}\omega \tag{3}$$

Then, the matched excitation waveform is chosen as in proportion to the unit impulse response reversed in time and shifted by t_0. This waveform can be represented by following[9]

$$x(t) = h_y(t_0 - t)/K \tag{4}$$

In the case of a linear system, the maximum response is in proportion to $1/K$.

Consider now the maximum response generated by the matched excitation waveform. The Fourier transform of Eq. (4) gives

$$X(\omega) = (1/K)e^{-i\omega t_0}H_y(-\omega) = (1/K)H_y^*(\omega)e^{-i\omega t_0} \tag{5a}$$

$$H_y(\omega) = Ke^{-i\omega t_0}X(-\omega) = KX^*(\omega)e^{-i\omega t_0} \tag{5b}$$

Substituting Eq. (5b) into Eq. (1), the response of the airplane is

$$y(t) = \frac{1}{2\pi}\int_{-\infty}^{\infty} KX^*(\omega)X(\omega)e^{i\omega(t-t_0)}\,\mathrm{d}\omega \tag{6}$$

Considering the exponential in the integrand, it is seen that the maximum response occurs at $t = t_0$.

$$y_{\max} = y(t_0) = K\left[\frac{1}{2\pi}\int_{-\infty}^{\infty} X^*(\omega)X(\omega)\,\mathrm{d}\omega\right] = K\sigma_x^2 \tag{7}$$

The value of the standard deviation does not change by the operations of a shift and reversal in time. Therefore from Eq. (4), there is a relationship between the standard deviations of the matched excitation waveform and the impulse response, that is,

$$\sigma_x = \sigma_{h_y}\big/K \tag{8}$$

Substituting Eq. (8) into Eq. (7) gives

$$y_{\max} = \sigma_{h_y}^2\big/K \tag{9}$$

Choosing the arbitrary constant to be $K = \sigma_{h_y}$, Eq. (9) is finally

$$y_{\max} = \sigma_{h_y} \tag{10}$$

σ_x also becomes one from Eq. (8). This result clearly shows that the matched excitation waveform with a constraint of a unit standard deviation leads to the maximum response σ_{h_y} at the time of t_0. This constraint is very important to compare the results of MFT with those for other gust inputs.

The von Kármán gust impulse response in Fig. 1 is then

$$g(t) = \frac{1}{2\pi}\int_{-\infty}^{\infty} G(\omega)e^{i\omega t}\,\mathrm{d}\omega \tag{11}$$

In addition, the critical gust profile is given by

$$w_g(t) = \frac{1}{2\pi}\int_{-\infty}^{\infty} W_g(\omega)e^{i\omega t}\,\mathrm{d}\omega \tag{12}$$

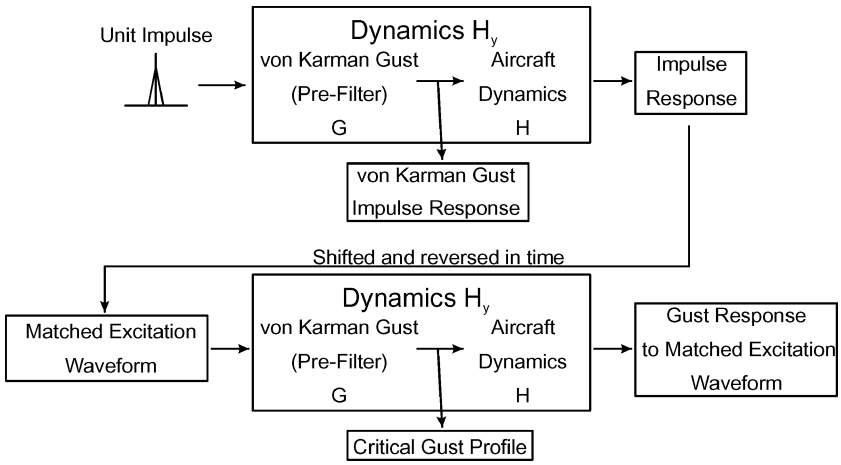

Fig. 1 Signal flow diagram of MFT.

where, using Eq. (5a),

$$W_g(\omega) = G(\omega)X(\omega) = \left(1/\sigma_{h_y}\right)G(\omega)H_y^*(\omega)e^{-i\omega t_0} \tag{13}$$

Next, consider the case of an arbitrary excitation waveform. $X'(\omega)$ is used instead of the matched excitation waveform. Equation (1) becomes

$$Y'(\omega) = H_y(\omega)X'(\omega) \tag{14}$$

From Eq. (6), then, the response of the airfoil is given by

$$y'(t) = \frac{1}{2\pi}\int_{-\infty}^{\infty} \sigma_{h_y} X^*(\omega)X'(\omega)e^{i\omega(t-t_0)}\,\mathrm{d}\omega \tag{15}$$

Applying the Schwartz's inequality to Eq. (15) gives

$$|y'(t)|^2 \le \sigma_{h_y}^2\left[\frac{1}{2\pi}\int_{-\infty}^{\infty} X^*(\omega)X(\omega)\,\mathrm{d}\omega\right] \times \left[\frac{1}{2\pi}\int_{-\infty}^{\infty} X'^*(\omega)X'(\omega)\,\mathrm{d}\omega\right] \tag{16}$$

Under the constraint of $\sigma_x = 1$,

$$|y'(t)| \le \sigma_{h_y} \tag{17}$$

Equation (17) makes it clear that any arbitrary excitation waveform cannot produce a larger response than the one which is caused by the matched excitation waveform.

Formulation of Analytical/Numerical Model

A numerical model has been formulated to obtain the dynamics. A typical airfoil section with a control surface is used for the structual model in this paper. The Wagner and the Küssner functions are employed for the unsteady aerodynamics model. Then, the combination of the structural model and unsteady aerodynamics gives the airplane dynamics. The gust is given by the von Kármán gust prefilter. Flutter and gust response analyses are based on these models.

Structural Model

A typical airfoil section with a control surface is shown in Fig. 2, which has three degrees of freedom (h, α, and β). The equations of motion of this model excited by the gust are derived from the Lagrange's equation and written as[18]

$$m\ddot{h} + S_\alpha\ddot{\alpha} + S_\beta\ddot{\beta} + m\omega_h^2 h = L^M + L^G \tag{18a}$$

$$S_\alpha\ddot{h} + I_\alpha\ddot{\alpha} + [I_\beta + b(a-e)S_\beta]\ddot{\beta} + I_\alpha\omega_\alpha^2\alpha = M_\alpha^M + M_\alpha^G \tag{18b}$$

$$S_\beta\ddot{h} + [I_\beta + b(a-e)S_\beta]\ddot{\alpha} + I_\beta\ddot{\beta} + I_\beta\omega_\beta^2\beta = M_\beta^M + M_\beta^G \tag{18c}$$

The lift caused by wing motion is composed of L_C^M and L_{NC}^M.

$$L^M = L_{\mathrm{NC}}^M + L_C^M = -\pi\rho b^2[U\dot{\alpha} + \ddot{h} - be\ddot{\alpha} - (1/\pi)UT_4\dot{\beta} - (1/\pi)T_1 b\ddot{\beta}] - 2\pi\rho bUC(k)w_{0.75c} \tag{19}$$

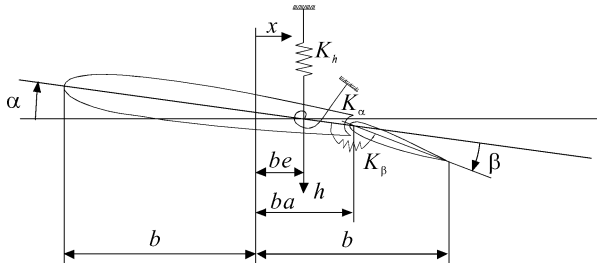

Fig. 2 Schematic of typical airfoil section with control surface.

Similarly, moments caused by wing motion are also comprised of circulatory and noncirculatory terms and are given by

$$M_\alpha^M = -\rho b^2\left\{\pi\left(\tfrac{1}{2}-e\right)Ub\dot{\alpha} + \pi\left(\tfrac{1}{8}+e^2\right)b^2\ddot{\alpha} + (T_4+T_{10})U^2\beta + \left[T_1 - T_8 - (a-e)T_4 + \tfrac{1}{2}T_{11}\right]Ub\dot{\beta} - [T_7 + (a-e)T_1]b^2\ddot{\beta} - \pi be\ddot{h}\right\} + 2\pi\rho b^2 U\left(\tfrac{1}{2}+e\right)C(k)w_{0.75c} \tag{20}$$

$$M_\beta^M = -\rho b^2\left\{\left[-2T_9 - T_1 + T_4\left(-\tfrac{1}{2}+e\right)\right]bU\dot{\alpha} + 2T_{13}b^2\ddot{\alpha} + (1/\pi)(T_5 - T_4T_{10})U^2\beta - (1/2\pi)T_4T_{11}bU\dot{\beta} - (1/\pi)T_3b^2\ddot{\beta} - T_1b\ddot{h}\right\} - \rho T_{12}b^2UC(k)w_{0.75c} \tag{21}$$

In Eqs. (19–21), $C(k)$ is the Theodorsen's function and $k = b\omega/U$ is the reduced frequency. The downwash at the 75% chord is given by

$$w_{0.75c}(t) = U\alpha + \dot{h} + b\left(\tfrac{1}{2}-e\right)\dot{\alpha} + (1/\pi)T_{10}U\beta + (1/2\pi)bT_{11}\dot{\beta} \tag{22}$$

Aerodynamic coefficients T_1 through T_{13} depend on the location of the elastic axis and the control surface hinge line and are shown in the Appendix.

In the case of the typical airfoil section without flap, the equations of motion can be obtained by substituting $\beta(t) = 0$ into Eqs. (18a) and (18b) and eliminating Eq. (18c). This is used for analyses in the limit $\omega_\beta \to \infty$.

Unsteady Aerodynamic Model

Aerodynamics caused by an indicial angle attack can be described by the Wagner function

$$\phi(\tau) = \frac{1}{2\pi i}\int_{-\infty}^{\infty}\frac{C(k)}{k}e^{ik\tau}\,\mathrm{d}k \tag{23}$$

The R. T. Jones approximation[19] to the Wagner function is often used for a gust study[20,21] and is also used in this paper,

$$\phi(\tau) = b_0 - b_1e^{-\beta_1\tau} - b_2e^{-\beta_2\tau} \tag{24}$$

The Laplace transform of Eq. (24) is

$$\bar{\phi} = \frac{b_0}{p} - \frac{b_1}{p+\beta_1} - \frac{b_2}{p+\beta_2} = \frac{1}{p} - \frac{0.165}{p+0.0455} - \frac{0.335}{p+0.300} \tag{25}$$

The bar symbol denotes the Laplace transform. The aerodynamics caused by arbitrary motion are then described by employing the Duhamel's integral:

$$L_C^M(\tau) = -2\pi\rho bUC(k)w_{0.75c} = -2\pi\rho Ub \times\left[w_{0.75c}(0)\phi(\tau) + \int_0^\tau \frac{\mathrm{d}w_{0.75c}(\sigma)}{\mathrm{d}\sigma}\phi(\tau-\sigma)\,\mathrm{d}\sigma\right] \tag{26}$$

The moments M_α^M and M_β^M can be obtained in the same way.

In a similar way, aerodynamics caused by an indicial gust can be described by the Küssner function.

$$\psi(\tau) = \frac{1}{2\pi i}\int_{-\infty}^{\infty}\frac{\{C(k)[J_0(k) - iJ_1(k)] + iJ_1(k)\}e^{ik(\tau-1)}}{k}\,\mathrm{d}k \tag{27}$$

Again an approximation can be applied to Eq. (27) and written in the Laplace domain as

$$\bar{\psi} = \frac{1}{p} - \frac{0.500}{p+0.130} - \frac{0.500}{p+1.000} \tag{28}$$

The lift caused by an arbitrary gust is described by employing the Duhamel's integral

$$L^G(\tau) = 2\pi\rho bU\left[w_G(0)\psi(\tau) + \int_0^\tau \frac{\mathrm{d}w_G(\sigma)}{\mathrm{d}\sigma}\psi(\tau-\sigma)\,\mathrm{d}\sigma\right] \tag{29}$$

Similarly, the aerodynamic moment about the elastic axis is

$$M_\alpha^G(\tau) = \left(\tfrac{1}{2}+e\right)bL^G(\tau) \tag{30}$$

The aerodynamic moment about the control surface hinge caused by gust is

$$M_\beta^G(\tau) = -\int_{ba}^{b} \Delta\bar{p}_a(x)e^{ik\tau}(x-ba)\,\mathrm{d}x \tag{31}$$

where $\Delta\bar{p}_a$ is given by the Schwarz' solution.[19]

$$\frac{\Delta\bar{p}_a(x^*)}{\rho U} = \frac{2}{\pi}[1-C(k)]\sqrt{\frac{1-x^*}{1+x^*}}\int_{-1}^{1}\sqrt{\frac{1+\xi^*}{1-\xi^*}}\bar{w}_G(\xi^*)e^{-ikx^*}\,\mathrm{d}\xi^*$$
$$+\frac{2}{\pi}\int_{-1}^{1}\left(\sqrt{\frac{1-x^*}{1+x^*}}\sqrt{\frac{1+\xi^*}{1-\xi^*}}\frac{1}{x^*-\xi^*}\right.$$
$$\left.-\frac{ik}{2}\,\ell_n\frac{1-x^*\xi^*+\sqrt{1-\xi^{*2}}\sqrt{1-x^{*2}}}{1-x^*\xi^*-\sqrt{1-\xi^{*2}}\sqrt{1-x^{*2}}}\right)\bar{w}_G(\xi^*)e^{-ikx^*}\,\mathrm{d}\xi^* \tag{32}$$

Describing Eq. (31) by using the Küssner function is complicated. Assuming $k \ll 1$, upwash caused by gust can be assumed to be constant over the wing. The circulatory part of aerodynamics caused by wing motion is then the same as aerodynamics caused by gust. Using downwash at 75% chord in the circulatory part of Eq. (21), w_G can be approximated as

$$w_G = -w_{0.75c} \tag{33}$$

Then, M_β^G is described by the Wagner function and the Duhamel's integral

$$M_\beta^G = \rho T_{12}b^2U\left[w_G(0)\phi(\tau) + \int_0^\tau \frac{\mathrm{d}w_G(\sigma)}{\mathrm{d}\sigma}\phi(\tau-\sigma)\,\mathrm{d}\sigma\right] \tag{34}$$

It has also been found that by neglecting M_β^G altogether the subsequently described numerical results are virtually unchanged.

Gust Model

The von Kármán power spectral density for a vertical gust[22] is given by

$$\Phi(\omega) = \sigma_g^2\frac{L}{2\pi U}\frac{1+(8/3)(1.339\omega L/U)^2}{[1+(1.339\omega L/U)^2]^{11/6}} \tag{35}$$

The corresponding form of the transfer function[23] for the von Kármán gust is

$$G(s) = \sigma_g\sqrt{\frac{L}{\pi U}}$$
$$\times\frac{[1+2.618\,(L/U)\,s][1+0.1298\,(L/U)\,s]}{[1+2.083\,(L/U)\,s][1+0.823\,(L/U)\,s][1+0.0898\,(L/U)\,s]} \tag{36}$$

Note that the following relationship between the Laplace variables s and p is used to obtain $G(p)$:

$$s = bp/U \tag{37}$$

Final Description of Equations of Motion

Assuming no motion and no gust on the wing at $\tau = 0$, the initial conditions are

$$w_{0.75c}(0) = 0, \qquad w_G(0) = 0 \tag{38}$$

The final description of equations of motion is obtained by nondimensionalization, transform of Eq. (18) to the Laplace domain, and substituting Laplace transformed Eqs. (19–22), (25), (26), (28), and (29–34) with the initial condition equation (38). In the matrix form, the equation is given by

$$[\mathbf{A}]\{\bar{\mathbf{x}}\} = \bar{w}_G\{\mathbf{b}\} \tag{39}$$

The elements of the matrix $\boldsymbol{A}$ are given in the Appendix.

Flutter Characteristics

This section of the paper describes the flutter characteristics of the model. Assuming no structural damping, the flutter equation is given by setting at $\boldsymbol{b} = 0$ in Eq. (39). Then the nontrivial solution is given by the determinant of $\boldsymbol{A}$:

$$\det[\boldsymbol{A}(p)] = 0 \tag{40}$$

The flutter calculation is executed for a range of the control surface natural frequency ω_β, from 5 to 120 rad/s. For the flutter and the gust-response calculation described in next section, the following values are set: $b = 1.143$ m, $e = 0.0$, $a = 0.5$, $m = 35.21$ kg, $I_\alpha = b^2m/3$ kg·m^2, $I_\beta = b^2m/48$ kg·m^2, $S_\alpha = 0.0$, $S_\beta = bm/16$ kg·m, $\omega_h = 29.09$ rad/s, $\omega_\alpha = 80.00$ rad/s, and $\rho = 1.2256$ kg/m^3. Some values are chosen from Ref. 24.

Shown in Fig. 3a is the flutter speed as a function of ω_β. As ω_β increases, the flutter speed approaches the asymptotic value (137 m/s) for the case of a wing with two degrees of freedom. It is found that the flutter speed becomes lowest at $\omega_\beta = 20$. However, structural damping can significantly increase this minimum flutter speed. Figure 3b shows the natural frequency as a function of airspeed at $\omega_\beta = 60$. It is known that this flutter is coupling between the first and the second mode.

Gust-Response Characteristics

Two kinds of gust responses have been computed. One is the response from the MFT. The other is the response to the one-minus-cosine gust. Then the gust responses obtained by both approaches are compared.

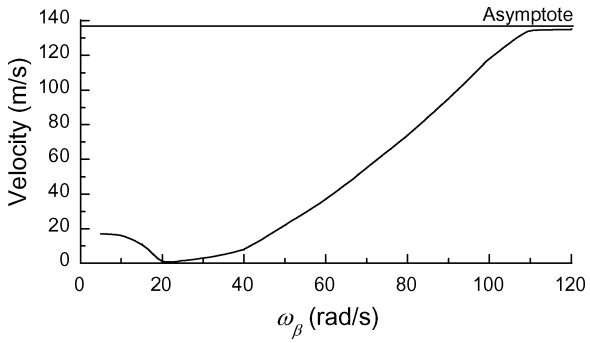

Fig. 3a Flutter speed vs control surface natural frequency.

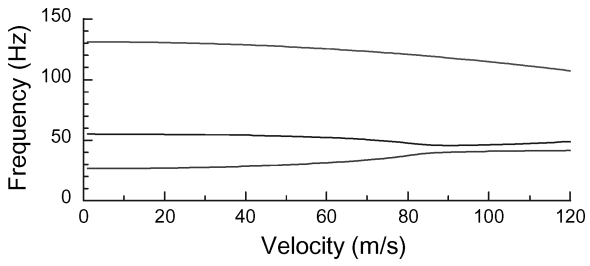

Fig. 3b Frequency vs airspeed.

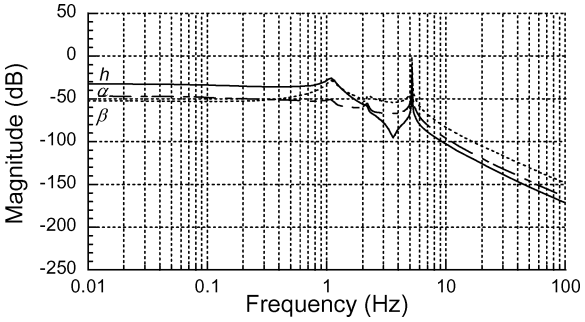

Fig. 4 Frequency responses of H_h, H_α, and H_β

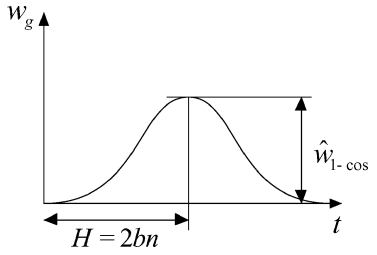

Fig. 5 One-minus-cosine gust profile.

Matched-Filter-Theory Approach

A transfer function is derived from Eq. (39).

$$\boldsymbol{H} = (1/\bar{w}_G)\{\bar{\boldsymbol{x}}\} = \boldsymbol{A}^{-1}\boldsymbol{b} \tag{41}$$

Using the transfer function for the von Kármán gust in Eq. (36), the total dynamics shown in Eq. (2) becomes

$$\boldsymbol{H}_y = G\boldsymbol{H} = \{H_h \quad H_\alpha \quad H_\beta\}^T \tag{42}$$

Here, the gust properties are set at $L = 762$ m, $\sigma_g = 1.0$ m/s, and the airspeed is $U = 28.6$ m/s. At this airspeed, it is found that flutter does not occur above $\omega_\beta = 55$ from Fig. 3. The frequency responses for dynamics $\boldsymbol{H}_y$ at $\omega_\beta = 60$ are shown in Fig. 4. It is clearly found that there is a peak near the natural frequency of the plunging motion ($\omega_h = 29.09$ rad/s $= 4.63$ Hz).

The impulse response of the plunging motion is selected here to obtain the matched excitation waveform:

$$h_y(\tau) = \mathcal{L}^{-1}(H_h) \tag{43}$$

The shift time is set at $\tau_0 = 80$ in Eq. (4), which is enough time for the impulse response to decay.

One-Minus-Cosine Discrete Gust

A one-minus-cosine gust profile is the gust structure shown in Fig. 5 and Eq. (44). This profile is an idealization of a real gust:

$$w_{1-\cos} = \begin{cases} \dfrac{1}{2}\hat{w}_{1-\cos}\left(1 - \cos\dfrac{2\pi t U}{2H}\right) & \\ = \dfrac{1}{2}\hat{w}_{1-\cos}\left(1 - \cos\dfrac{\pi\tau}{2n}\right) & (0 \le \tau \le 4n) \\ 0 & (4n < \tau) \end{cases} \tag{44}$$

The standard deviation value should be appropriately chosen to compare with the result of the MFT, that is, the standard deviations of one-minus-cosine gust and the critical gust profile should be same. The ratio of the standard deviation of the critical gust profile to that of the matched excitation waveform is given by

$$R = \frac{\sigma_{w_g}}{\sigma_x} = \frac{\sqrt{\int_{-\infty}^{\infty} w_g^2(\tau)\,\mathrm{d}\tau}}{\sqrt{\int_{-\infty}^{\infty} x^2(\tau)\,\mathrm{d}\tau}} \tag{45}$$

But this ratio is equal to the standard deviation of the critical gust profile σ_{w_g} because of the constraint $\sigma_x = 1$. The standard deviation of the gust profile presented by Eq. (44) is

$$\sigma_{1-\cos} = \sqrt{\int_{-\infty}^{\infty} w_{1-\cos}^2(\tau)\,\mathrm{d}\tau} = \sqrt{\frac{3n}{2}}\hat{w}_{1-\cos} \tag{46}$$

Then, the appropriate one-minus-cosine gust profile is given by

$$w_{1-\cos}(\tau) = R \times \frac{w_{1-\cos}(\tau)}{\sigma_{1-\cos}} = \sqrt{\frac{1}{6n}}R\left(1 - \cos\frac{\pi\tau}{2n}\right) \tag{47}$$

Note that if $n \to 0$

$$w_{1-\cos}(\tau) = R \times \delta(\tau) \tag{48}$$

Using the selected gust profile of Eq. (47), a direct comparison with the MFT result can be made.

The gradient distance is yet unknown. For static gust loads, the gradient distance is selected to be 12.5 mean geometric wing chords in the U.S. Air Force, U.S. Navy, and Federal Aviation Administration requirements.[25,26] However, here the gust gradient distance is selected to give maximum response because the dynamic response is very sensitive to the gradient distance.[27] The maximum response of the plunging motion is shown as a function of gradient distance in Fig. 6. It is found that the response becomes a maximum at $n = 1.1$. As a result of computations, it is found that the maximum response occurs at the same gradient distance for the full range of ω_β considered. Thus, the one-minus-cosine gust is considered for $n = 1.1$.

Results and Discussion

Shown in Fig. 7 are worst-case gust responses of the plunging motion h at $\omega_\beta = 60$. The critical gust profile, the matched exciting waveform, and the one-minus-cosine gust profile are all shown

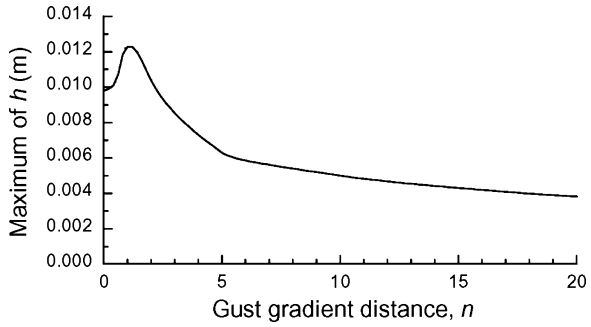

Fig. 6 One-minus-cosine gust response vs gust gradient distance.

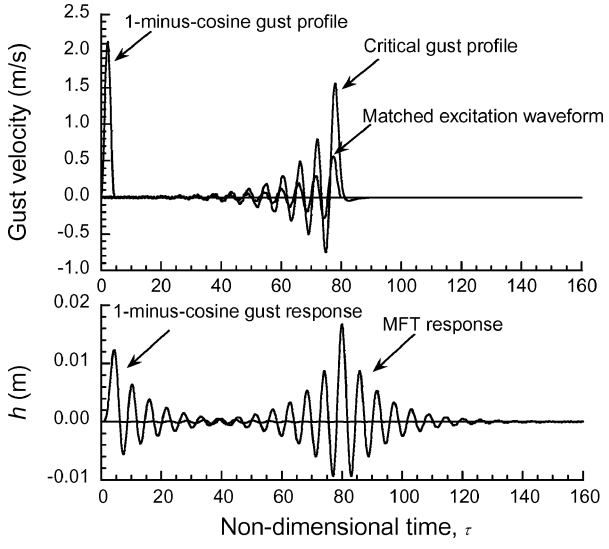

Fig. 7 Gust profiles and responses.

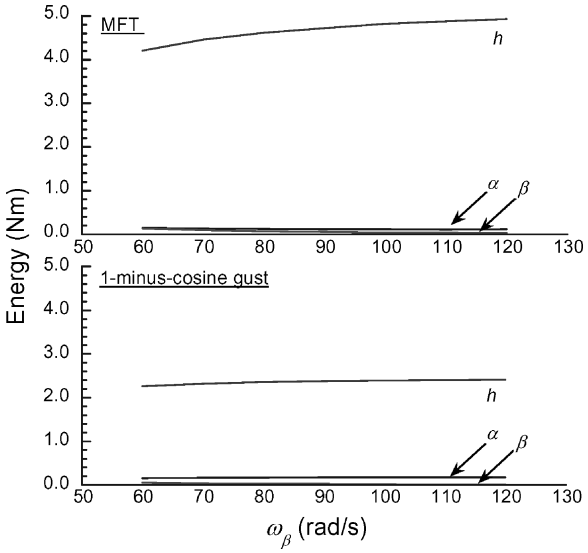

Fig. 8 Energy of maximum response as a function of ω_β.

together. It is found that the response calculated by the MFT becomes maximum at $\tau_0 = 80$. The maximal value 0.0167 is equal to the standard deviation σ_{h_y} and also the constant K. These results prove that the theory is appropriately applied to the model. Compared with the one-minus-cosine gust response, the response by the MFT is larger for the chosen response variable h. The energy of maximum responses in h, α, and β as a function of ω_β are shown in Fig. 8. The total energy in h, α, and β are respectively given by $m\omega_h^2 h^2/2$, $I_\alpha \omega_\alpha^2 \alpha^2/2$, and $I_\beta \omega_\beta^2 \beta^2/2$. Note that kinetic energy becomes zero at a time of maximum response. It is clear that the energy in the h motion is larger than for α and β motion in both methods. This is because the worst-case gust that maximizes the h motion is selected. Results have indicated that the energy in the h motion by using the MFT is about twice as large as that by using the one-minus-cosine gust. Moreover, using the MFT it is possible to obtain directly the worst-case gust responses. In contrast, the one-minus-cosine gust response is more difficult to obtain (more computationally expensive) and also underestimates the worst-case gust responses.

Next, consider characteristics of the worst-case gust responses as a function of hinge stiffness. The energy found by the MFT measurably decreases with decreasing ω_β. Hence, it is found that a change in hinge stiffness changes the energy of the motion h that occurs as a result of the worst-case gust. In contrast, the response energy obtained by using the one-minus-cosine gust is almost constant, and the one-minus-cosine gust therefore cannot evaluate the effect of the hinge stiffness appropriately.

Conclusions

The worst-case gust response for a typical airfoil section with a control surface has been computed using matched filter theory (MFT). MFT can obtain directly the maximum responses without tuning the gust excitation and/or the use of the calculus of variations. Determination of the gust response has focused on motion instead of loads in the present work. The equation of motion for an airfoil plus control surface with three degrees of freedom has been formulated, and the unsteady aerodynamics are modeled by the Wagner and the Küssner functions. A prefilter has used the von Kármán gust transfer function.

Maximum responses calculated by the MFT are compared with those determined by the one-minus-cosine gust. The one-minus-cosine gust needs to be tuned by an appropriate selection of a gradient distance. It has been shown that the MFT response is about twice that of the one-minus-cosine gust for the plunging motion. Thus it is clear that the MFT can be effectively applied to determine the worst-case gust. Second, the characteristics of gust responses as a function of hinge stiffness have been examined. The results show that the energy of the plunging motion that occurs as a result of the worst-case gust measurably decreases with decreasing hinge stiffness.

The effectiveness of the MFT has been shown in this paper. Also, these results will be useful to an understanding of how to control aircraft motion caused by a gust.

Appendix: Coefficients and Matrix

Aerodynamic Coefficients

Aerodynamic coefficients T_i included in Eqs. (19–22) are given as[28]

$$T_1 = -\left(\tfrac{1}{3}\right)\sqrt{1-a^2}(2+a^2) + a\cos^{-1}a$$

$$T_2 = a(1-a^2) - \sqrt{1-a^2}(1+a^2)\cos^{-1}a + a(\cos^{-1}a)^2$$

$$T_3 = \left(\tfrac{1}{8}+a^2\right)(\cos^{-1}a)^2 + \left(\tfrac{1}{4}\right)a\sqrt{1-a^2}\cos^{-1}a(7+2a^2) - \left(\tfrac{1}{8}\right)(1-a^2)(5a^2+4)$$

$$T_4 = -\cos^{-1}a + a\sqrt{1-a^2}$$

$$T_5 = -(1-a^2) - (\cos^{-1}a)^2 + 2a\sqrt{1-a^2}\cos^{-1}a$$

$$T_6 = T_2$$

$$T_7 = -\left(\tfrac{1}{8}+a^2\right)\cos^{-1}a + \left(\tfrac{1}{8}\right)a\sqrt{1-a^2}(7+2a^2)$$

$$T_8 = -\left(\tfrac{1}{3}\right)\sqrt{1-a^2}(2a^2+1) + a\cos^{-1}a$$

$$T_9 = \left(\tfrac{1}{2}\right)\left[\left(\tfrac{1}{3}\right)\left(\sqrt{1-a^2}\right)^3 + aT_4\right]$$

$$T_{10} = \sqrt{1-a^2} + \cos^{-1}a$$

$$T_{11} = \cos^{-1}a(1-2a) + \sqrt{1-a^2}(2-a)$$

$$T_{12} = \sqrt{1-a^2}(2+a) - \cos^{-1}a(2a+1)$$

$$T_{13} = \left(\tfrac{1}{2}\right)[-T_7 - (a-e)T_1]$$

Matrix A

Elements a_{ij} of $\boldsymbol{A}$, which is a 3×3 matrix in Eq. (39), are given as follows:

$$a_{11} = m(U^2/b^2)p^2 + m\omega_h^2 + \pi\rho U^2(1+2\bar{\phi})p^2$$

$$a_{12} = S_\alpha(U^2/b^2)p^2 + \pi\rho bU^2(1+2\bar{\phi})p + \pi\rho bU^2[(1-2e)\bar{\phi} - e]p^2$$

$$a_{13} = S_\beta(U^2/b^2)p^2 + \rho bU^2(2T_{10}\bar{\phi} - T_4) + \rho bU^2(T_{11}\bar{\phi} - T_1)p^2$$

$$a_{21} = S_\alpha(U^2/b^2)p^2 - \pi\rho bU^2[(1+2e)\bar{\phi} + e]p^2$$

$$a_{22} = I_\alpha(U^2/b^2)p^2 + I_\alpha\omega_\alpha^2 + \pi\rho b^2U^2\left[\left(\tfrac{1}{2}-e\right) - (1+2e)\bar{\phi}\right]p + \pi\rho b^2U^2\left[\tfrac{1}{8} + e^2 - \left(\tfrac{1}{2}-2e^2\right)\bar{\phi}\right]p^2$$

$$a_{23} = [I_\beta + b(a-e)S_\beta](U^2/b^2)p^2 + \rho b^2U^2(T_4+T_{10}) + \rho b^2U^2\left[-(1+2e)T_{10}\bar{\phi} + T_1 - T_8 - (a-e)T_4 + \tfrac{1}{2}T_{11}\right]p + \rho b^2U^2\left[-\left(\tfrac{1}{2}+e\right)T_{11}\bar{\phi} - T_7 - (a-e)T_1\right]p^2$$

$$a_{31} = S_\beta(U^2/b^2)p^2 + \rho bU^2(T_{12}\bar{\phi} - T_1)p^2$$

$$a_{32} = [I_\beta + b(a-e)S_\beta](U^2/b^2)p^2 + \rho b^2U^2\left[T_{12}\bar{\phi} - 2T_9 - T_1 - \left(\tfrac{1}{2}-e\right)T_4\right]p + \rho b^2U^2\left[\left(\tfrac{1}{2}-e\right)T_{12}\bar{\phi} + 2T_{13}\right]p^2$$

$$a_{33} = I_\beta (U^2/b^2)p^2 + I_\beta \omega_\beta^2 + (1/\pi)\rho b^2 U^2 (T_5 - T_4 T_{10})$$
$$+ (1/\pi)\rho b^2 U^2 \left(T_{10} T_{12} \bar{\phi} - \tfrac{1}{2} T_4 T_{11}\right)$$
$$+ (1/\pi)\rho b^2 U^2 \left(\tfrac{1}{2} T_{10} T_{12} \bar{\phi} - T_3\right) p^2$$

References

[1]Taylor, J., *Manual of Aircraft Loads*, AGARDograph 83, Pergamon, New York, 1965, Chap. 10.

[2]Etkin, B., "Turbulent Wind and Its Effect on Flight," *Journal of Aircraft*, Vol. 18, No. 5, 1981, pp. 327–345.

[3]Noback, R., "Comparison of Discrete and Continuous Gust Methods for Airplane Design Loads Determination," *Journal of Aircraft*, Vol. 23, No. 3, 1986, pp. 226–231.

[4]Poirion, F., "Response of an Airplane to Non-Gaussian Atmospheric Turbulence," *Journal of Aircraft*, Vol. 28, No. 9, 1991, pp. 579–583.

[5]Jones, J. G., "Statistical Discrete Gust Theory for Aircraft Loads," Royal Aircraft Establishment, RAE TR-73167, Farnborough, England, U.K., Dec. 1973.

[6]Jones, J. G., "Statistical-Discrete-Gust Method for Predicting Aircraft Loads and Dynamic Response," *Journal of Aircraft*, Vol. 26, No. 4, 1989, pp. 382–398.

[7]Papoulis, A., "Maximum Response with Energy Constraints and the Matched Filter Principle," *IEEE Transactions on Circuit Theory*, Vol. CT-17, No. 2, 1970, pp. 175–182.

[8]Zeiler, T. A., and Pototzky, A. S., "On the Relationship Between Matched Filter Theory as Applied to Gust Loads and Phased Design Loads Analysis," NASA CR 181802, April 1989.

[9]Pototzky, A. S., Zeiler, T. A., and Perry, B., III, "Calculating Time-Correlated Gust Loads Using Matched Filter and Random Process Theories," *Journal of Aircraft*, Vol. 28, No. 5, 1991, pp. 346–352.

[10]Scott, R. C., Pototzky, A. S., and Perry, B., III, "Determining Design Gust Loads for Nonlinear Aircraft—Similarity Between Methods Based on Matched Filter Theory and on Stochastic Simulation," NASA TM 107614, April 1992.

[11]Scott, R. C., Pototzky, A. S., and Perry, B., III, "Computation of Maximized Gust Loads for Nonlinear Aircraft Using Matched-Filter-Based Schemes," *Journal of Aircraft*, Vol. 30, No. 5, 1993, pp. 763–768.

[12]Scott, R. C., Pototzky, A. S., and Perry, B., III, "Matched-Filter and Stochastic-Simulation-Based Methods of Gust Loads Prediction," *Journal of Aircraft*, Vol. 32, No. 5, 1995, pp. 1047–1055.

[13]Zeiler, T. A., "Matched Filter Concept and Maximum Gust Loads," *Journal of Aircraft*, Vol. 34, No. 1, 1997, pp. 101–108.

[14]Gilholm, K., and Watson, G. H., "Prediction of Time-Correlated Gust Loads Using an Incremental Stochastic Search," *Journal of Aircraft*, Vol. 36, No. 5, 1999, pp. 792–801.

[15]Lee, Y. N., and Lan, C. E., "Analysis of Random Gust Response with Nonlinear Unsteady Aerodynamics," *AIAA Journal*, Vol. 38, No. 8, 2000, pp. 1305–1312.

[16]Ueda, T., Matsushita, H., Suzuki, S., and Miyazawa, Y., "ACT Wind-Tunnel Experiments of a Transport-Type Wing," *Journal of Aircraft*, Vol. 28, No. 2, 1991, pp. 139–145.

[17]Suzuki, S., and Yonezawa, S., "Simultaneous Structure/Control Design Optimization of a Wing Structure with a Gust Load Alleviation System," *Journal of Aircraft*, Vol. 30, No. 2, 1993, pp. 268–274.

[18]Fung, Y. C., *An Introduction to the Theory of Aeroelasticity*, Dover, New York, 1993, Chap. 6.

[19]Bisplinghoff, R. L., Ashley, H., and Halfman, R. L., *Aeroelasticity*, Addison Wesley Longman, Cambridge, MA, 1955, Chap. 5.

[20]Kholodar, D. B., and Dowell, E. H., "The Influence of a Nonzero Angle of Attack and Gust Loads on the Nonlinear Response of a Typical Airfoil Section with a Control Surface Freeplay," *International Journal of Nonlinear Sciences and Numerical Simulation*, Vol. 1, No. 3, 2000, pp. 153–165.

[21]Marzocca, P., Librescu, L., and Chiocchia, G., "Aeroelastic Response of 2-D Lifting Surfaces to Gust and Arbitrary Explosive Loading Signatures," *International Journal of Impact Engineering*, Vol. 25, No. 1, 2001, pp. 41–65.

[22]Etkin, B., *Dynamics of Atmospheric Flight*, Wiley, New York, 1972, Chap. 13.

[23]Barr, N. M., Gangsaas, D., and Schaeffer, D. R., "Wind Tunnel Models for Flight Simulator Certification of Landing and Approach Guidance and Control Systems," Boeing Commercial Airplane Co., Final Rept. FAA-RD-74-206, Seattle, WA, Dec. 1974.

[24]Sears, W. R., and Sparks, B. O., "On the Reaction of an Elastic Wing to Vertical Gust," *Journal of the Aeronautical Sciences*, Vol. 9, No. 2, 1941, pp. 64–67.

[25]Noback, R., "Review and Comparison of Discrete and Continuous Gust Methods for the Determination of Airplane Design Loads," National Aerospace Lab., Rept. NLR TR82134U, Amsterdam, 1982.

[26]Flomenhoft, H. I., "Brief History of Gust Models for Aircraft Design," *Journal of Aircraft*, Vol. 31, No. 5, 1994, pp. 1225–1227.

[27]Hoblit, F. M., *Gust Loads on Aircraft: Concepts and Applications*, AIAA Education Series, AIAA, Washington, DC, 1988, Chap. 3.

[28]Theodorsen, T., "General Theory of Aerodynamic Instability and the Mechanism of Flutter," NACA Rept. No. 496, 1935.